

**Constraints on
aerosol processes in
climate models**

Z. Kipling et al.

**Constraints on aerosol processes in
climate models from vertically-resolved
aircraft observations of black carbon**

**Z. Kipling¹, P. Stier¹, J. P. Schwarz^{2,3}, A. E. Perring^{2,3}, J. R. Spackman^{2,3},
G. W. Mann^{4,5}, C. E. Johnson⁶, and P. J. Telford^{7,8}**

¹Department of Physics, University of Oxford, UK

²Co-operative Institute for Research in Environmental Sciences, University of Colorado,
Boulder, Colorado, USA

³Chemical Sciences Division, Earth System Research Laboratory, National Oceanic and
Atmospheric Administration, Boulder, Colorado, USA

⁴National Centre for Atmospheric Science, University of Leeds, UK

⁵School of Earth and Environment, University of Leeds, UK

⁶Met. Office Hadley Centre, Exeter, UK

⁷National Centre for Atmospheric Science, University of Cambridge, UK

⁸Department of Chemistry, University of Cambridge, UK

Received: 28 November 2012 – Accepted: 4 December 2012 – Published: 7 January 2013

Correspondence to: Z. Kipling (kipling@atm.ox.ac.uk)

Published by Copernicus Publications on behalf of the European Geosciences Union.

[Title Page](#)

[Abstract](#) [Introduction](#)

[Conclusions](#) [References](#)

[Tables](#) [Figures](#)

[⏪](#) [⏩](#)

[◀](#) [▶](#)

[Back](#) [Close](#)

[Full Screen / Esc](#)

[Printer-friendly Version](#)

[Interactive Discussion](#)



Abstract

Evaluation of the aerosol schemes in current climate models is dependent upon the available observational data. In-situ observations from flight campaigns can provide valuable data about the vertical distribution of aerosol that is difficult to obtain from satellite or ground-based platforms, although they are localised in space and time. Using single-particle soot-photometer (SP2) measurements from the HIAPER Pole-to-Pole Observations (HIPPO) campaign, which consists of many vertical profiles over a large region of the Pacific, we evaluate the meridional and vertical distribution of black carbon (BC) aerosol simulated by the HadGEM3-UKCA and ECHAM5-HAM2 models. Both models show a similar pattern of overestimating the BC column burden compared to that derived from the observations, in many areas by an order of magnitude. However, by sampling the simulated BC mass mixing ratio along the flight track and comparing to the observations, we show that this discrepancy has a rather different vertical structure in the two models.

Using this methodology, we conduct sensitivity tests on two specific elements of the models: biomass-burning emissions and scavenging by convective precipitation. We show that, by coupling the convective scavenging more tightly with convective transport, both the column burden and vertical distribution of BC in HadGEM3-UKCA are significantly improved with respect to the observations, demonstrating the importance of a realistic representation of this process. In contrast, updating from GFED2 to GFED3.1 biomass-burning emissions makes a more modest improvement in both models, which is not statistically significant.

We also demonstrate the important role that nudged simulations (where the large-scale model dynamics are continuously relaxed towards a reanalysis) can play in this type of evaluation, allowing statistically significant differences between configurations of the aerosol scheme to be seen where the differences between the corresponding free-running simulations would not be significant.

ACPD

13, 437–473, 2013

Constraints on aerosol processes in climate models

Z. Kipling et al.

Title Page

Abstract

Introduction

Conclusions

References

Tables

Figures

⏪

⏩

◀

▶

Back

Close

Full Screen / Esc

Printer-friendly Version

Interactive Discussion



1 Introduction

Aerosol particles in the atmosphere play an important role in the climate system on both global and regional scales, through several mechanisms: direct modification of the short-wave radiation budget by scattering and absorption (Ångström, 1962; Schulz et al., 2006; Myhre et al., 2012); effects on clouds and the hydrological cycle, indirectly modifying the radiation budget (Twomey, 1977; Albrecht, 1989; Lohmann and Feichter, 2005); and “semi-directly” by altering the temperature profile of the atmosphere, and evaporating or suppressing cloud, through absorption of radiation (Hansen, 1997; Koch and Del Genio, 2010). The magnitudes of all these effects are subject to considerable uncertainty.

Black carbon (BC) aerosol can contribute to all of these classes of effect, although its absorption of short-wave radiation makes it of particular interest in the context of the direct and semi-direct effects (Stier et al., 2007; Ramanathan and Carmichael, 2008). The relative magnitudes of these effects, and thus the sign of the net (semi-)direct forcing due to BC, are thought to depend heavily on the vertical distribution of BC, and in particular its altitude relative to cloud layers (Zarzycki and Bond, 2010). In addition, “aged” BC particles with a soluble coating can act as cloud condensation nuclei (Penner et al., 1996; Lohmann et al., 2000) and thus contribute to indirect effects; ageing may also reduce the lifetime of black carbon (by increasing susceptibility to wet deposition) and enhance its absorption of radiation (Ackerman and Toon, 1981; Stier et al., 2006; Schwarz et al., 2008).

Some progress has been made in analysing the relative positions of BC and cloud layers, and the resulting radiative effects, from satellite observations (Peters et al., 2011; Wilcox, 2012). However, neither passive satellite remote sensing nor ground-based observations can provide well-resolved vertical profiles of BC (or aerosol in general), and thus we turn to in-situ aircraft observations. Although such observations are limited in spatial and temporal coverage, they can provide data with much better vertical resolution than can be obtained from other sources, as well as more direct

Constraints on aerosol processes in climate models

Z. Kipling et al.

Title Page

Abstract

Introduction

Conclusions

References

Tables

Figures

⏪

⏩

◀

▶

Back

Close

Full Screen / Esc

Printer-friendly Version

Interactive Discussion



measurements of the quantities (e.g. concentrations, mixing ratios, composition and particle size distributions) represented in aerosol models.

Previous studies using aircraft observations to evaluate aerosol models on a global scale have generally compared monthly-mean model profiles with campaign-mean profiles from a collection of separate campaigns (which may differ in their methodology), each over a limited geographical area (e.g. Koch et al., 2009). Other studies have focused on more detailed evaluation on a regional scale using individual flight campaigns – e.g. Reddington et al. (2012), which also highlights the importance of uncertainties in the size distribution of BC as well as its total mass.

The large-scale flight campaign conducted by the High-performance Instrumented Airborne Platform for Environmental Research (HIAPER) Pole-to-Pole Observations (HIPPO) of Carbon Cycle and Greenhouse Gases Study (Wofsy et al., 2011) provides the opportunity to evaluate against consistently-collected data from a single campaign over a large area of the Pacific region. The data are described in more detail in Sect. 2. The BC data from the first phase of the HIPPO campaign are analysed in Schwarz et al. (2010), where the observed vertical profiles are used to evaluate the simulated BC profiles from the Aerosol Comparisons between Observations and Models (AEROCOM; <http://dataipsl.ipsl.jussieu.fr/AEROCOM>) Phase I (Textor et al., 2006) models, comparing climatological monthly-mean model profiles against regional-mean profiles from HIPPO. The model diversity is large – one to two orders of magnitude over a wide altitude range, both in the Pacific regions studied in Schwarz et al. (2010) and the continental regions in Koch et al. (2009) – but both the mean and median of the model ensemble systematically overestimate the BC mass mixing ratio (MMR) compared to the observations.

In this study, we carry out a more detailed evaluation of the vertical distribution of BC in two particular models, HadGEM3–UKCA and ECHAM5–HAM2, against BC mass mixing ratio data derived from the first three phases of the HIPPO campaign. These models and their configurations are described in Sect. 3. Rather than averaging the instantaneous observations on a regional basis and comparing to model climatology,

Constraints on aerosol processes in climate models

Z. Kipling et al.

Title Page

Abstract

Introduction

Conclusions

References

Tables

Figures

◀

▶

◀

▶

Back

Close

Full Screen / Esc

Printer-friendly Version

Interactive Discussion



we use nudging and interpolation techniques to sample the models in time and space along the track of the flight campaign, as described in Sect. 4.

We apply this approach to investigate and constrain the effects of convective scavenging (which has an important role in controlling vertical transport) and biomass-burning emissions (which are the most temporally and spatially variable source of BC) on the vertical profile of BC in the models. To this end, we conduct a series of sensitivity tests, as described in Sect. 5, to assess how the agreement with the observations is affected by the choice of convective scavenging scheme and emissions inventory.

2 Observational data

There have been five phases of the HIPPO campaign completed (<http://hippo.ucar.edu/>); data from the first three (in January 2009, October/November 2009 and March/April 2010) were available in time for this analysis. Each phase consists of an approximate meridional transect over the Pacific, with detours into neighbouring continental regions – the flight tracks can be seen in Fig. 1. Along each track, a series of fairly regular ascents and descents were made, providing vertically-resolved measurements, typically spanning 300 m above the surface to 8.5 km a.s.l. with some profiles extending to ~ 14 km. In total, we identify 184 separate vertical profiles suitable for our analysis (the criteria used are discussed in Sect. 4.1).

A wide range of instruments were carried on these flights, but for our purposes the most relevant data comes from a Single Particle Soot Photometer (SP2; Schwarz et al., 2006), which measures the mass of BC in individual aerosol particles. Particles were detected within a range of ~ 0.8 to 175 fg BC (~ 75 to 540 nm volume-equivalent diameter, assuming a void-free density of $1.8 \times 10^3 \text{ kg m}^{-3}$).

Constraints on aerosol processes in climate models

Z. Kipling et al.

Title Page

Abstract

Introduction

Conclusions

References

Tables

Figures

◀

▶

◀

▶

Back

Close

Full Screen / Esc

Printer-friendly Version

Interactive Discussion



Following Schwarz et al. (2010), we calculate the MMR of BC in the atmosphere by aggregating the observed particles over 1-min intervals:

$$m_{\text{BC}} = 1.1 \frac{F}{\rho_{\text{air}}} \sum_{i=1}^N M_i, \quad (1)$$

where (M_1, \dots, M_N) are the masses of BC in each individual particle observed by the SP2 instrument, F is the volumetric flow rate at which the air is sampled ($4\text{cm}^3\text{s}^{-1}$, constant) and ρ_{air} is the density of the sampled air, derived from contemporaneous measurements of ambient pressure from the HIPPO flight data, and a fixed temperature of 290K representing the cabin air temperature of the aircraft. (These are an approximation of the actual sampling conditions, but the resulting error is small compared to that from other sources.) The factor of 1.1 inflates the mass by 10% to account for the portion of the aerosol size spectrum which the instrument does not detect, as per Schwarz et al. (2010). We then produce a “curtain” plot of BC MMR against latitude and altitude to show the distribution of BC over a vertical slice through the atmosphere (top row of Fig. 2). We attach an uncertainty of $\pm 30\%$ to these MMR values (the $\pm 40\%$ quoted in the above paper is now considered overly cautious). However, there may be some additional sampling uncertainty in the cleanest regions where only a small number of particles are detected per minute; however this is not considered further in this analysis.

With the exception of HIPPO-2, which makes a detour to Australia at about 30°S , there is generally more BC seen in the northern hemisphere than the Southern Hemisphere at all levels (which is consistent with the greater anthropogenic emissions in the north) – this contrast is particularly stark for HIPPO-3, which spent very little time near land. While some BC is seen in the lower and mid tropical troposphere, very little is seen at higher levels (above about 6km) in the tropics in any of the phases; at higher latitudes, however, significant BC mass mixing ratios frequently extend into the upper troposphere.

Constraints on aerosol processes in climate models

Z. Kipling et al.

Title Page

Abstract

Introduction

Conclusions

References

Tables

Figures

⏪

⏩

◀

▶

Back

Close

Full Screen / Esc

Printer-friendly Version

Interactive Discussion



3 Models

Two aerosol–climate models are considered here: HadGEM3–UKCA and ECHAM5–HAM2. These are described in the following sections, and the major differences relevant to black carbon aerosol are summarised in Table 1.

3.1 HadGEM3–UKCA

HadGEM3 (Hewitt et al., 2010) is the latest version of the Hadley Centre Global Environmental Model developed at the UK Met. Office. Although the full model contains many components (atmosphere, land surface, ocean, sea ice etc.), this study is concerned only with the uncoupled atmosphere component, using prescribed sea-surface temperature (SST) and sea ice fields. The dynamical core (Davies, 2005) is non-hydrostatic and fully compressible, with semi-Lagrangian advection and a hybrid sigma/height vertical coordinate. Large-scale cloud uses the bulk prognostic scheme of Wilson et al. (2008), with precipitation microphysics based on Wilson and Ballard (1999); sub-grid-scale convection is based on the mass-flux scheme of Gregory and Rowntree (1990) with subsequent modifications.

The standard tropospheric chemistry scheme in UKCA (O'Connor et al., 2012) is used. This includes oxidants (O_x , HO_x and NO_x) and hydrocarbons (CO, ethane and propane) with eight emitted species, 102 gas-phase reactions, 27 photolytic reactions and interactive wet and dry deposition. An additional aerosol-precursor chemistry scheme treats the oxidation of sulphur compounds (SO_2 and dimethyl sulphide) and monoterpene to form the sulphuric acid and organic compounds which may condense to form secondary aerosol material.

The aerosol scheme in UKCA (Mann et al., 2012) is the two-moment modal version of the Global Model of Aerosol Processes (GLOMAP-mode; Mann et al., 2010), which follows the M7 framework (Vignati, 2004) in transporting five components (sulphate, sea salt, black carbon, particulate organic matter and mineral dust) in seven internally-mixed log-normal modes (four soluble and three insoluble; not all components are

Constraints on aerosol processes in climate models

Z. Kipling et al.

Title Page

Abstract

Introduction

Conclusions

References

Tables

Figures

◀

▶

◀

▶

Back

Close

Full Screen / Esc

Printer-friendly Version

Interactive Discussion



Constraints on aerosol processes in climate models

Z. Kipling et al.

Title Page

Abstract

Introduction

Conclusions

References

Tables

Figures

⏪

⏩

◀

▶

Back

Close

Full Screen / Esc

Printer-friendly Version

Interactive Discussion



found in all modes). Because mineral dust is transported by a separate scheme (Woodward, 2001) in HadGEM3, only four components and five modes are enabled in the UKCA configuration of GLOMAP-mode used here (omitting the two larger insoluble modes which contain only mineral dust). The representation of aerosol microphysical processes is based on the sectional GLOMAP-bin scheme (Spracklen et al., 2005), with each process acting sequentially in an operator-split manner (except nucleation, coagulation and condensation which are solved iteratively).

Primary BC emissions use the AEROCOM recommended size distributions (Dentener et al., 2006), as modified by Stier et al. (2005), but with biofuel emissions using the same distribution as fossil fuel rather than biomass burning. Fossil-fuel and biofuel emissions are added to the lowest model level with a geometric mean diameter of 60 nm, while biomass-burning emissions have a geometric mean diameter of 150 nm and are distributed uniformly in height over levels 2 to 12 (~ 50 m to 3 km, compressed over orography) – this is different to the TOMCAT-based version of GLOMAP-MODE documented in Mann et al. (2010), which uses the biome-dependent vertical profiles recommended in Dentener et al. (2006). For all sources, the geometric standard deviation of the particle diameter is 1.59.

BC aerosol is initially insoluble, but can be “aged” into the soluble Aitken mode following uptake of sulphuric acid and secondary organic material via condensation and coagulation. This ageing proceeds at a rate consistent with a 10-monolayer coating being required to make a particle soluble.

Both soluble and insoluble particles may be removed by dry deposition and below-cloud impaction scavenging; soluble particles may also be removed by in-cloud nucleation scavenging. Dry deposition and gravitational sedimentation are calculated following Slinn (1982) and Zhang et al. (2001). Below-cloud scavenging follows Slinn (1984), using Beard and Grover (1974) scavenging coefficients and terminal velocities from Easter and Hales (1983), assuming a modified Marshall-Palmer raindrop size distribution (Sekhon and Srivastava, 1971). In-cloud scavenging assumes that 100 % of the aerosol in the soluble accumulation and coarse modes is taken up by cloud water in

Constraints on aerosol processes in climate modelsZ. Kipling et al.

[Title Page](#)[Abstract](#)[Introduction](#)[Conclusions](#)[References](#)[Tables](#)[Figures](#)[⏪](#)[⏩](#)[◀](#)[▶](#)[Back](#)[Close](#)[Full Screen / Esc](#)[Printer-friendly Version](#)[Interactive Discussion](#)

the cloudy fraction of each 3-D grid box, and is then removed at the same rate at which the large-scale cloud water is converted to rain. Aerosol is removed immediately, and is not returned to the atmosphere when rain evaporates. Convective rainfall is treated similarly, but assumes a cloud fraction of 30 % and a conversion rate of 99 % over 6 h in all grid-boxes where convective rain is produced. (This is different to the TOMCAT-based version of GLOMAP-mode, in which convective scavenging is dependent on the rain rate while large-scale scavenging uses a fixed removal timescale.) The scavenged aerosol is removed from the grid-box mean tracers after the convection scheme has run – i.e. from the post-convection environmental air, rather than the convective up-draught itself. This allows a greater separation of the convection and aerosol schemes, but may limit the ability of convective scavenging to control vertical transport (as we show in Sect. 6.1).

The model configuration used here is based on a development version of HadGEM3 (atmosphere-only, climatological SST, Met. Office Unified Model version 7.3) at N96L38 resolution (1.25° latitude \times 1.875° longitude \times 38 vertical levels up to ~ 40 km) with UKCA in a standard tropospheric chemistry and aerosol configuration as described above, with aerosol feedbacks disabled. The large-scale model dynamics are nudged towards ERA-Interim (Dee et al., 2011) reanalysis data, following Telford et al. (2008, 2012). Free-running simulations (without nudging) were also run for comparison.

For the sensitivity tests, four different simulations were carried out covering the period of the first three phases of the HIPPO campaign, as shown in Table 2. All simulations were run from September 2008 through to the end of April 2010, allowing four months spin-up before the start of HIPPO-1.

The BASE configuration is derived from the standard UKCA aerosol configuration, which takes its black carbon emissions from the AEROCOM hindcast inventory (Diehl et al., 2012), including emissions from fossil fuel, biofuel and biomass burning through to the end of 2006. Although the HIPPO campaign began after this, the fossil fuel and biofuel emissions have little interannual variability and so we simply repeat those for 2006. Biomass burning, however, has significant interannual variability; since the

emissions inventory does not cover the required period, we used a monthly climatology derived from the “modern” portion of the AEROCOM hindcast inventory (1997 to 2006), which is based on monthly-mean emission fields of the Global Fire Emissions Database (GFED) version 2 (van der Werf et al., 2006). Other (non-BC) emissions are also taken from year 2006 of the AEROCOM hindcast inventory, or (for additional gas-phase emissions not included therein but required by the UKCA chemistry scheme) from year 2006 of Representative Concentration Pathway (RCP) 8.5 (Riahi et al., 2011).

3.2 ECHAM5–HAM2

ECHAM5 (Roeckner et al., 2003) is the fifth-generation climate model developed at the Max Planck Institute for Meteorology. It has a spectral dynamical core, solving prognostic equations for vorticity, divergence, surface pressure and temperature in spherical harmonics with a triangular truncation. A hybrid sigma/pressure vertical coordinate is used. Physical parameterisations are solved on a corresponding Gaussian grid. Tracer transport is semi-Lagrangian in grid-point space (Lin and Rood, 1996).

HAM 2.0 (Stier et al., 2005; Zhang et al., 2012) is also a two-moment modal aerosol scheme based on the M7 framework (Vignati, 2004), transporting five components (sulphate, sea salt, black carbon, particulate organic matter and mineral dust) in seven internally-mixed log-normal modes (four soluble and three insoluble). Unlike in UKCA, mineral dust in ECHAM5–HAM2 is incorporated into the M7 framework.

Primary BC emissions use a modified version of the AEROCOM recommended size distributions, accounting for the width of the M7 modes. Fossil-fuel and biofuel emissions are added as a surface flux to the boundary-layer vertical diffusion equations, while biomass-burning emissions use a biome-dependent vertical profile, as specified for AEROCOM Phase I (Dentener et al., 2006). BC aerosol is initially insoluble, but can be “aged” by sulphate through condensation and coagulation to become soluble; in contrast to UKCA only a single monolayer is required.

Dry deposition of soluble and insoluble particles follows Ganzeveld et al. (1998), modified to use the explicit size distribution from the model, and is applied as a surface

Constraints on aerosol processes in climate models

Z. Kipling et al.

Title Page

Abstract

Introduction

Conclusions

References

Tables

Figures

◀

▶

◀

▶

Back

Close

Full Screen / Esc

Printer-friendly Version

Interactive Discussion



Constraints on aerosol processes in climate modelsZ. Kipling et al.

[Title Page](#)[Abstract](#)[Introduction](#)[Conclusions](#)[References](#)[Tables](#)[Figures](#)[◀](#)[▶](#)[◀](#)[▶](#)[Back](#)[Close](#)[Full Screen / Esc](#)[Printer-friendly Version](#)[Interactive Discussion](#)

flux to the boundary-layer vertical diffusion along with the emissions. Below-cloud scavenging is calculated according to the rain and snow fluxes, using size-dependent collection efficiencies from Seinfeld and Pandis (1998). In-cloud scavenging removes a prescribed fraction of the number and mass of aerosol in each mode from the cloudy part of each grid box at the same rate at which large-scale cloud water/ice is converted to rain/snow. Scavenging in convective clouds is coupled with the tracer transport in the mass-flux convection scheme, and proceeds similarly but removing aerosol from the convective tracer flux according to the rate at which water and ice are removed in convective precipitation. Where (a fraction of) the precipitation in a column evaporates before reaching the ground, the same fraction of the aerosol removed from the column is returned to the atmosphere.

Large-scale cloud follows the two-moment scheme of Lohmann et al. (2007) with modifications by Lohmann and Hoose (2009) and Abdul-Razzak and Ghan (2000) aerosol activation (Stier et al., 2012), with Sundqvist et al. (1989) cloud cover. Convection follows the mass-flux scheme of Tiedtke (1989), with modifications by Nordeng (1994).

The model configuration used here is based on ECHAM 5.5 (atmosphere-only, AMIP2 prescribed SST) at T63L31 resolution ($\sim 1.875^\circ \times 31$ vertical levels up to ~ 10 hPa) with HAM 2.0. Once again, the large-scale dynamics are nudged towards ERA-Interim (Dee et al., 2011) reanalysis data.

For the sensitivity tests, four different simulations were carried out for the period covering the first three phases of the HIPPO campaign, as shown in Table 2. As for HadGEM3–UKCA, all simulations were run from September 2008 through to the end of April 2010, allowing four months spin-up before the start of HIPPO-1.

In the BASE configuration, emissions are taken from the AEROCOM hindcast inventory (Diehl et al., 2012) for 2006, with biomass-burning emissions using a 1997 to 2006 climatology as described for HadGEM3–UKCA.

4 Method

As mentioned in Sect. 1, to best compare to the aircraft measurements from the HIPPO campaign, we sample the output of the HadGEM3–UKCA and ECHAM5–HAM2 models along the flight track. However, to give a general indication of how the models' BC distributions compare to the observations, we first show regional maps of the simulated BC column burden with that derived from the SP2 measurements over-plotted along the flight track.

4.1 Burdens

From a modelling perspective, column-integrated mass burdens are a useful metric by which to measure the distribution of aerosol. However, it is difficult to obtain direct measurements of aerosol burden on large scales, as satellite-based instruments can only measure integrated optical properties (with passive instruments) or vertically-resolved backscatter (with active lidar). Burdens cannot be inferred from such measurements without additional knowledge of the chemical and microphysical properties of the aerosol particles. Ground-based sun-photometers and lidar are similarly limited, while ground-based in-situ measurements are limited to particles near the surface. The geographical and vertical coverage of the HIPPO campaign, however, provides a basis on which to evaluate model burdens directly.

We estimate the local BC column burden in the vicinity of each HIPPO ascent or descent profile. Suitable profiles are identified as periods of near-continuous ascent or descent covering at least the 0.5km to 7.5km altitude range. From each profile, the mean BC concentration (mass of BC per unit volume) in each 0.5km altitude interval from 0 to 15km is calculated. These are then integrated vertically to give an estimate of the column burden (shown on the maps in Fig. 1 as coloured circles).

Because the HIPPO profiles do not extend all the way to the surface or our 15km "lid", there is some uncertainty in how we extrapolate the profile when calculating the burden. We calculate a lower estimate by assuming the BC concentration is zero outside

Constraints on aerosol processes in climate models

Z. Kipling et al.

Title Page

Abstract

Introduction

Conclusions

References

Tables

Figures

◀

▶

◀

▶

Back

Close

Full Screen / Esc

Printer-friendly Version

Interactive Discussion



the altitude range of the observations; for an upper estimate, we assume that the BC concentrations observed at the bottom and top of the profile continue to the surface and 15 km respectively. (This does not give a true upper bound on the burden, since the concentrations outside the observed altitude range may be higher than those within, but provides an estimate of the extrapolation uncertainty.) Because Schwarz et al. (2010) attribute the largest part of the $\pm 30\%$ uncertainty in BC MMR to calibration (correlated) rather than random (uncorrelated) error, we assume that the full $\pm 30\%$ may apply to the derived burden estimates. These ranges (including both the extrapolation and measurement uncertainty) are shown as the red bars on the side-plots in Fig. 1.

4.2 Point-by-point comparison

For a more detailed point-by-point comparison, we perform on-line interpolation of the instantaneous mass mixing ratio fields from each model to the points along the HIPPO flight track, following O'Connor et al. (2005) and Telford et al. (2012). The spatial interpolation is linear in log-pressure and both horizontal directions. Temporally, each observation is matched to the following model time-step. Coupled with nudging to reproduce the observed synoptic conditions (notwithstanding the uncertainty in reanalysis fields in remote regions with sparse observations), this allows us to sample the model output consistently with the observations rather than using a monthly mean or climatology.

Once this sampling has been done, we can evaluate the model output pointwise against the actual HIPPO observations both visually and quantitatively. For a visual comparison we simply plot the differences in mass mixing ratio at each point on the flight track. For a more quantitative analysis, we look at the mean difference (bias) and correlation coefficient between the logarithms of the real and simulated mass mixing ratios, over all the points along the flight track. (Logarithms are taken as the distribution of observed mixing ratios appears to be approximately log-normal; this results in a distribution which is more symmetric and closer to a normal distribution, making standard statistical techniques more meaningful. Without logarithms, the correlation coefficient is distorted by differences in the long upper tail of the distribution.)

Constraints on aerosol processes in climate models

Z. Kipling et al.

Title Page

Abstract

Introduction

Conclusions

References

Tables

Figures

◀

▶

◀

▶

Back

Close

Full Screen / Esc

Printer-friendly Version

Interactive Discussion



Constraints on aerosol processes in climate modelsZ. Kipling et al.

[Title Page](#)[Abstract](#)[Introduction](#)[Conclusions](#)[References](#)[Tables](#)[Figures](#)[⏪](#)[⏩](#)[◀](#)[▶](#)[Back](#)[Close](#)[Full Screen / Esc](#)[Printer-friendly Version](#)[Interactive Discussion](#)

To estimate the uncertainty in the quantitative analysis, we use bootstrapping to construct 95 % confidence intervals for the bias and correlation. Because both the observed and modelled data series show significant autocorrelation, we use a moving-block bootstrap (Kunsch, 1989) with block length 30 (i.e. resampling in approximately half-hour blocks). This provides an estimate of the uncertainty due to random sampling variability. To incorporate the uncertainty in the SP2-derived mixing ratios, we extend the error bars on the bias by $\pm 30\%$ (to accommodate the worst-case effect on the bias, of a systematic calibration error). For the correlation, we apply random multiplicative Gaussian white noise with a standard deviation of 30 % to each bootstrap sample (to accommodate the worst case effect on the correlation, of completely uncorrelated observation errors).

There is some additional uncertainty in the comparison, due to the limited size range of the SP2 measurements – we adjust the measurements as described in Sect. 2 to account for this, but some uncertainty remains as in practice the fraction of BC which is within the detectable range will be variable. An alternative approach, of calculating the number of modelled particles which would contain a detectable amount of BC, is problematic because the models assume uniform composition, with BC mass spread over all particles in a given mode. This results in lower BC masses per particle, and many fewer detectable particles, than if the BC is confined to a subset of particles – which Reddington et al. (2012) show may indeed be the case, at least in the more polluted air over continental Europe.

5 Sensitivity tests

5.1 Biomass-burning emissions

One of the most variable and uncertain sources of BC is from biomass burning (responsible for approximately half the BC emissions by mass in the models, the remainder coming from fossil fuel and biofuel burning). The emissions used in the BASE

configurations of both models are a monthly climatology derived from the AEROCOM hindcast inventory, itself based on the Global Fire Emissions Database (GFED), version 2 (van der Werf et al., 2006). However, GFED version 3.1 is now available (van der Werf et al., 2010). Amongst various improvements to the emission estimates, there is a substantial reduction in total carbon emissions from biomass burning, which is reflected in the BC emissions. In addition, GFED3.1 provides daily fractional emission fields (at the same 0.5° resolution as the monthly data, but not resolved by chemical species) which can be applied to each month's data to estimate emissions at daily time resolution, and a diurnal profile for each month (also at 0.5° resolution, in 3-h intervals), giving estimates at 3-hourly time resolution (Mu et al., 2011). The new dataset now covers the period to the end of 2010, sufficient for simulations during the first three phases of the HIPPO campaign and removing the need to extrapolate the emission dataset. Switching to GFED3.1 emissions for biomass burning gives the G3M (monthly emissions) and G3H (3-hourly emissions) configurations (the latter only implemented in ECHAM5–HAM2).

In HadGEM3–UKCA, both BASE and G3M configurations distribute the biomass-burning emissions uniformly in height over levels 2 to 12 (~ 50m to 3km). In ECHAM5–HAM2, the BASE configuration uses a biome-dependent vertical profile for the emissions, as in AEROCOM Phase I (Dentener et al., 2006), while the G3M and G3H configurations divide the emissions equally between the model levels diagnosed to be within the boundary layer.

5.2 Convective scavenging

Convection plays a dominant role in the upward transport of both gaseous and particulate matter in the atmosphere, with wide variation amongst models especially for short-lived species (Hoyle et al., 2011). However, convection (especially the vigorous, deep convection that can transport air parcels from the boundary layer to the upper troposphere) is also associated with intense precipitation, and thus a significant amount of material may be removed by wet scavenging before it is detrained from the convective

Constraints on aerosol processes in climate models

Z. Kipling et al.

Title Page

Abstract

Introduction

Conclusions

References

Tables

Figures

◀

▶

◀

▶

Back

Close

Full Screen / Esc

Printer-friendly Version

Interactive Discussion



updraught. Schwarz et al. (2010) identify the treatment of this process as likely to be a major factor in the diversity of the AEROCOM models and their high bias compared to the HIPPO-1 SP2 observations, particularly in the tropics.

The models used here take two different approaches to convective scavenging. In the operator-split approach, as used in the BASE configuration of HadGEM3–UKCA, convective scavenging removes aerosol from the grid-box mean field after the convection scheme (including convective tracer transport) has run. In the in-plume approach, as used in ECHAM5–HAM2, aerosol is removed directly from the tracer flux in the convective updraught, along with the removal of water by convective precipitation. Additional simulations with HadGEM3–UKCA have also been carried out using an in-plume scheme (CVSCAV and CVSCAV+G3M configurations). This assumes that 100% of the soluble accumulation and coarse modes in the upward convective tracer flux is taken up by the cloud drops and therefore removed in proportion to the amount of cloud water which precipitates (as in the existing scheme for large-scale cloud); additionally, 50% (by mass and number) of the soluble Aitken mode is taken up and removed, as a crude representation of the fact that smaller particles can be activated in the faster updraughts found in convective cloud. (The figure of 50% is somewhat arbitrary, and there is certainly scope for refinement – both the large-scale and convective schemes should ideally use an appropriate critical radius based on Köhler theory.) It should be noted, however, that this scheme does not yet include resuspension of aerosol when rain evaporates (nor does the existing operator-split scheme, or the large-scale scavenging scheme), unlike that in ECHAM5–HAM2.

6 Results

6.1 HadGEM3–UKCA

The BC MMR from HadGEM3–UKCA (in its BASE configuration), sampled at 1-min intervals along the flight track for the first three phases of the HIPPO campaign, is

Constraints on aerosol processes in climate models

Z. Kipling et al.

Title Page

Abstract

Introduction

Conclusions

References

Tables

Figures

◀

▶

◀

▶

Back

Close

Full Screen / Esc

Printer-friendly Version

Interactive Discussion



shown in the second row of Fig. 2. Although some features (e.g. the disparity between the hemispheres in the HIPPO-3 data) are well reproduced, the model does not appear to reproduce other large-scale features of the observations very well. Most noticeably, for all three phases, the model has a significant excess of BC in the upper troposphere, especially in the tropics.

Figure 3 shows the difference between the HadGEM3–UKCA simulations in each configuration and the actual observations from each phase of the HIPPO campaign.

It is clear from these difference plots that, at least for HIPPO-1 and HIPPO-2, the upper-tropospheric excess seen in the BASE configuration is largely removed when the in-plume convective scavenging scheme is switched on (i.e. in CVSCAV and CVSCAV+G3M), suggesting that the lack of realistic convective scavenging may have been responsible. The third row of Fig. 2 shows the BC mixing ratio from the CVSCAV+G3M simulation, which is visibly more realistic with respect to the observations. For HIPPO-3, the improvement is largely confined to the Southern Hemisphere; in the Northern Hemisphere both simulations produce too little aerosol at lower levels and too much aloft. This is despite the fact that HIPPO-3 observed more BC at upper levels in the Northern Hemisphere than the earlier phases.

The change in switching to GFED3.1 biomass-burning emissions (i.e. BASE to G3M) is less dramatic. While, for HIPPO-1 and HIPPO-2, the difference plot for the G3M simulation indicates less of a positive bias than for BASE, the upper-tropospheric excess remains clear. Applying the emissions change on top of the in-plume convective scavenging (i.e. going from CVSCAV to CVSCAV+G3M) removes what little excess remains in the middle and upper troposphere, but appears to leave an overall negative bias compared to the observations. For HIPPO-3, the differences from the choice of emissions are less clear.

It thus appears that for HIPPO-1 and HIPPO-2 globally, and for HIPPO-3 in the Southern Hemisphere, the disagreement between the BASE model and observations is dominated by the lack of realistic convective scavenging, and is much improved when an in-plume approach is introduced. For HIPPO-3 in the Northern Hemisphere,

Constraints on aerosol processes in climate models

Z. Kipling et al.

Title Page

Abstract

Introduction

Conclusions

References

Tables

Figures

◀

▶

◀

▶

Back

Close

Full Screen / Esc

Printer-friendly Version

Interactive Discussion



however, it appears that the disagreement is dominated by other effects which have not yet been identified.

The differences can also be seen in the burdens (top two rows of Fig. 1). The BASE simulation over-predicts the BC burden at most of the profile locations, in many cases by an order of magnitude. CVSCAV+G3M performs much better, with the model burden frequently close to the range estimated from the HIPPO observations. For brevity, the separate plots for CVSCAV and G3M are omitted; however as before, most of the improvement is seen in the former and is particularly pronounced over the tropical warm pool region where strong convective scavenging is expected. The high burdens observed in the Arctic region have been attributed by Schwarz et al. (2010) to a localised biomass-burning plume, which the models cannot be expected to resolve.

6.2 ECHAM5–HAM2

The BC MMR from ECHAM5–HAM2 (in its BASE configuration), sampled at 1-min intervals along the flight track for the first three phases of the HIPPO campaign, is shown in the bottom row of Fig. 2. These do not exhibit the large upper-troposphere excesses seen in the HadGEM3–UKCA BASE simulation, but there are some unexpectedly large mixing ratios at even higher altitudes (including into the lower stratosphere).

Figure 4 shows the difference between the ECHAM5–HAM2 simulations in each configuration and the actual observations from each phase of the HIPPO campaign. The lower-stratosphere anomalies are clear in all simulations, and for HIPPO-1 and HIPPO-2 the BASE configuration shows patches of (mostly positive) bias throughout the troposphere that are not immediately obvious from Fig. 2.

Many of the strongest biases are reduced in the G3M simulation, suggesting that much of the tropospheric error in the BASE configuration may be attributable to the choice and implementation of biomass-burning emissions. It is possible that some of this difference is due to the different vertical profile of emissions between BASE and G3M. However, an additional simulation (not shown here) for HIPPO-1 with the same GFED2 emissions as BASE but the boundary-layer-following vertical profile of G3M

Constraints on aerosol processes in climate models

Z. Kipling et al.

Title Page

Abstract

Introduction

Conclusions

References

Tables

Figures

◀

▶

◀

▶

Back

Close

Full Screen / Esc

Printer-friendly Version

Interactive Discussion



shows results very similar to BASE. This suggests that it is the updated inventory, rather than the change in vertical profile, which makes the difference.

As in HadGEM3–UKCA (CVSCAV), HIPPO-3 looks rather different to the earlier phases. There appears to be little change between the ECHAM5–HAM2 BASE and G3M simulations, with the tropospheric error in both simulations dominated by negative anomalies throughout most of the Northern Hemisphere.

For all three phases, there is almost no visible difference between the G3M and G3H simulations. This indicates that, at least for simulations in remote regions such as those covered in the HIPPO campaign, monthly biomass-burning emissions are sufficient as any high-frequency variability at the source is smoothed out during transport. Higher-time-resolution emissions could provide more benefits for simulations closer to source regions, however.

The ECHAM5–HAM2 simulated burdens (third row of Fig. 1) show a similar pattern of overestimating the observations as the HadGEM3–UKCA BASE simulation, despite ECHAM5–HAM2 already having an in-plume convective scavenging scheme. Clearly in this case either the scavenging is nevertheless too weak, or some other process is responsible for the high burden in ECHAM5–HAM2. The AEROCOM Phase I (Textor et al., 2006) median model, shown in the bottom row, shows a similar positive bias.

The presence of high BC burdens in the remote Pacific in these models, in a way that does not correspond with observations, suggests that the model BC lifetime is too long. In HadGEM3–UKCA this appears to be a structural issue with convective scavenging; in ECHAM5–HAM2 and other models it may be due to different processes.

6.3 Quantitative evaluation

Figure 5 shows the bias and correlation coefficient of $\log(\text{BC MMR})$ for each simulation against each phase of the HIPPO campaign, along with bootstrap uncertainty estimates as described in Sect. 4.

The improvement in both bias and correlation when switching to in-plume convective scavenging in HadGEM3–UKCA can clearly be seen when going from BASE to CVS-

Constraints on aerosol processes in climate models

Z. Kipling et al.

Title Page

Abstract

Introduction

Conclusions

References

Tables

Figures

◀

▶

◀

▶

Back

Close

Full Screen / Esc

Printer-friendly Version

Interactive Discussion



CAV, or from G3M to CVSCAV+G3M (with the exception of the negative bias against HIPPO-2 and HIPPO-3 in the CVSCAV+G3M simulation). The improvement in correlation should perhaps be regarded as more relevant, as the bias is likely to be more susceptible to model tuning/calibration. For all three phases, this increase in correlation (0.22 → 0.41, 0.27 → 0.42, 0.51 → 0.65 between BASE and CVSCAV for HIPPO-1, -2, -3 respectively) is statistically significant in the sense that the error bars of the nudged BASE and CVSCAV (or G3M and CVSCAV+G3M) simulations do not overlap. Carrying out the analysis separately for the points in the two hemispheres (not shown) indicates that the increase in correlation comes largely from the Northern Hemisphere.

For both models, a small improvement in correlation (although not in bias for HadGEM3–UKCA CVSCAV) is seen when going from BASE to G3M (or CVSCAV to CVSCAV+G3M), although the overlapping error bars indicate that this is not statistically significant. As with the visual analysis, there is almost no difference between the ECHAM5–HAM2 G3M and G3H simulations. It is probably the case that evaluation closer to source regions would be more powerful in distinguishing between emissions inventories and their time resolution.

The correlation and, in most cases, also the bias are much improved in the nudged HadGEM3–UKCA simulations (solid symbols) compared to their free-running counterparts (hollow symbols). The correlation increases for the BASE configuration are 0.14 → 0.22, 0.08 → 0.27, 0.44 → 0.51 between free-running and nudged simulations for HIPPO-1, -2, -3 respectively. In addition, the improvement in bias and correlation from changes to the model configuration is enhanced in the nudged simulations. This is particularly significant for HIPPO-1, where nudging eliminates the overlapping error bars on the correlation axis between BASE and CVSCAV. This allows us to conclude that the improvement in CVSCAV is statistically significant, which may not have been clear from the free-running simulations alone. (It should be noted in this context that the error bars on the free-running models are an underestimate – ensemble simulations would be needed to quantify the additional uncertainty from the simulated meteorology.) Thus not only does nudging help to produce realistic simulations of aerosol

Constraints on aerosol processes in climate models

Z. Kipling et al.

Title Page

Abstract

Introduction

Conclusions

References

Tables

Figures

◀

▶

◀

▶

Back

Close

Full Screen / Esc

Printer-friendly Version

Interactive Discussion



during a given flight campaign, but it also makes it easier to evaluate the effect of changes to the aerosol scheme by damping errors due to differences in large-scale dynamics.

7 Conclusions

In this study, we develop methods for evaluating aerosol–climate models against large-scale aircraft campaigns, and apply these to investigate the impact of convective scavenging and biomass-burning emissions on the vertical profile of black carbon.

By running two aerosol–climate models in nudged configurations and interpolating their output onto the track of a flight campaign, we make a detailed pointwise comparison between model output and in-situ aircraft observations. Using data from a campaign such as HIPPO, which has good vertical resolution over an extended geographical area, this gives a powerful tool for evaluating the vertical distribution of aerosol in the models. We also show how these measurements can be used to evaluate column-integrated burdens in the models, which are a more direct product of most models than the optical/radiative properties (e.g. aerosol optical depth) which can be evaluated via remote sensing.

We apply this approach to black carbon aerosol in the HadGEM3–UKCA and ECHAM5–HAM2 models, and shown how each has different areas of disagreement with the HIPPO SP2 observations. Both models significantly over-predict BC burden, especially in the more remote regions, suggesting that the BC lifetime is too long. In the case of HadGEM3–UKCA, the largest discrepancy (an excess of aerosol in the tropical upper troposphere) can be eliminated by switching from the default operator-split convective scavenging scheme to one which scavenges directly from the convective plume. This change improves both the vertical distribution of BC and the simulated burdens against the HIPPO observations, yielding a statistically significant increase in the pointwise correlation coefficient for all three phases of the HIPPO campaign (0.22 → 0.41, 0.27 → 0.42, 0.51 → 0.65 for HIPPO-1, -2, -3 respectively).

Constraints on aerosol processes in climate models

Z. Kipling et al.

Title Page

Abstract

Introduction

Conclusions

References

Tables

Figures

⏪

⏩

◀

▶

Back

Close

Full Screen / Esc

Printer-friendly Version

Interactive Discussion



Constraints on aerosol processes in climate models

Z. Kipling et al.

Title Page

Abstract

Introduction

Conclusions

References

Tables

Figures

⏪

⏩

◀

▶

Back

Close

Full Screen / Esc

Printer-friendly Version

Interactive Discussion



In both models, a somewhat smaller and not statistically significant improvement can be seen when switching from GFED2-based biomass-burning emissions to GFED3.1; however there is virtually no change in this remote region when the time resolution of these emissions is increased from monthly to 3-hourly. It seems likely that a similar analysis with a wider range of flight campaigns, including the major biomass-burning regions, might better constrain the choice of such emissions.

We show for HadGEM3–UKCA that both the correlation between the BASE configuration and the observations, and the increase in correlation due to the new convective scavenging scheme, are enhanced when the simulations are nudged as opposed to free-running. In this way, nudging can enable statistically significant improvements in the model to be detected where they might not be in a free-running simulation; e.g. the above increase in the correlation of the nudged model against HIPPO-1 (from 0.22 to 0.41) is statistically significant, while the corresponding increase for the free-running model (from 0.14 to 0.27) is not.

It is clear that vertically-resolved in-situ measurements of aerosol have an important role to play in evaluating the aerosol distributions simulated by aerosol–climate models, in conjunction with satellite remote sensing and ground-based observations, and that they can provide particular insight into the processes governing the vertical transport of aerosol in the atmosphere, as we have seen with convective scavenging.

Acknowledgements. This work was supported by the Natural Environment Research Council [grant number NE/G006148/1]; and the Met. Office. HIPPO flight data provided by NCAR/EOL under sponsorship of the National Science Foundation (<http://data.eol.ucar.edu/>). ERA-Interim data provided by Paul Berrisford and the European Centre for Medium-Range Weather Forecasts (ECMWF). GFED3.1 biomass-burning emissions data provided by Guido van der Werf. AEROCOM median model data supplied by the AEROCOM project, from data provided by the contributing modellers. Computing resources provided by the Met. Office/NERC Joint Weather & Climate Research Programme (JWCRP) and Deutsche Klimarechenzentrum (DKRZ). Thanks to Nick Schutgens for a number of insightful discussions during the course of this work.

References

- Abdul-Razzak, H. and Ghan, S. J.: A parameterization of aerosol activation 2. multiple aerosol types, *J. Geophys. Res.*, 105, 6837–6844, 2000. 447
- Ackerman, T. P. and Toon, O. B.: Absorption of visible radiation in atmosphere containing mixtures of absorbing and nonabsorbing particles, *Appl. Optics*, 20, 3661–3667, 1981. 439
- Albrecht, B. A.: Aerosols, cloud microphysics, and fractional cloudiness, *Science*, 245, 1227–1230, 1989. 439
- Ångström, A.: Atmospheric turbidity, global illumination and planetary albedo of the earth, *Tellus*, 14, 435–450, doi:10.1111/j.2153-3490.1962.tb01356.x, 1962. 439
- Beard, K. V. and Grover, S. N.: Numerical Collision Efficiencies for Small Raindrops Colliding with Micron Size Particles, *J. Atmos. Sci.*, 31, 543–550, doi:10.1175/1520-0469(1974)031<0543:NCEFSR>2.0.CO;2, 1974. 444
- Davies, T.: A new dynamical core of the Met Office's global and regional modelling of the atmosphere, *Q. J. Roy. Meteor. Soc.*, 131, 1759–1782, doi:10.1256/qj.04.101, 2005. 443
- Dee, D. P., Uppala, S. M., Simmons, A. J., Berrisford, P., Poli, P., Kobayashi, S., Andrae, U., Balmaseda, M. A., Balsamo, G., Bauer, P., Bechtold, P., Beljaars, A. C. M., van de Berg, L., Bidlot, J., Bormann, N., Delsol, C., Dragani, R., Fuentes, M., Geer, A. J., Haimberger, L., Healy, S. B., Hersbach, H., Hólm, E. V., Isaksen, I., Kållberg, P., Köhler, M., Matricardi, M., McNally, A. P., Monge-Sanz, B. M., Morcrette, J.-J., Park, B.-K., Peubey, C., de Rosnay, P., Tavolato, C., Thépaut, J.-N., and Vitart, F.: The ERA-interim reanalysis: configuration and performance of the data assimilation system, *Q. J. Roy. Meteor. Soc.*, 137, 553–597, doi:10.1002/qj.828, 2011. 445, 447
- Dentener, F., Kinne, S., Bond, T., Boucher, O., Cofala, J., Generoso, S., Ginoux, P., Gong, S., Hoelzemann, J. J., Ito, A., Marelli, L., Penner, J. E., Putaud, J.-P., Textor, C., Schulz, M., van der Werf, G. R., and Wilson, J.: Emissions of primary aerosol and precursor gases in the years 2000 and 1750 prescribed data-sets for AeroCom, *Atmos. Chem. Phys.*, 6, 4321–4344, doi:10.5194/acp-6-4321-2006, 2006. 444, 446, 451, 467
- Diehl, T., Heil, A., Chin, M., Pan, X., Streets, D., Schultz, M., and Kinne, S.: Anthropogenic, biomass burning, and volcanic emissions of black carbon, organic carbon, and SO₂ from 1980 to 2010 for hindcast model experiments, *Atmos. Chem. Phys. Discuss.*, 12, 24895–24954, doi:10.5194/acpd-12-24895-2012, 2012. 445, 447

ACPD

13, 437–473, 2013

Constraints on aerosol processes in climate models

Z. Kipling et al.

Title Page

Abstract

Introduction

Conclusions

References

Tables

Figures

◀

▶

◀

▶

Back

Close

Full Screen / Esc

Printer-friendly Version

Interactive Discussion



Constraints on aerosol processes in climate models

Z. Kipling et al.

Title Page

Abstract

Introduction

Conclusions

References

Tables

Figures

◀

▶

◀

▶

Back

Close

Full Screen / Esc

Printer-friendly Version

Interactive Discussion



Easter, R. C. and Hales, J. M.: Interpretation of the OSCAR data for reactive gas scavenging, in: *Precipitation Scavenging, Dry Deposition, and Resuspension*, Elsevier, 649–662, 1983. 444

Ganzeveld, L., Lelieveld, J., and Roelofs, G.-J.: A dry deposition parameterization for sulfur oxides in a chemistry and general circulation model, *J. Geophys. Res.*, 103, 5679–5694, doi:10.1029/97JD03077, 1998. 446, 467

Gregory, D. and Rowntree, P. R.: A mass flux convection scheme with representation of cloud ensemble characteristics and stability-dependent closure, *Mon. Weather Rev.*, 118, 1483–1506, 1990. 443

Hansen, J.: Radiative forcing and climate response, *J. Geophys. Res.-Atmos.*, 102, 6831–6864, 1997. 439

Hewitt, H. T., Copsey, D., Culverwell, I. D., Harris, C. M., Hill, R. S. R., Keen, A. B., McLaren, A. J., and Hunke, E. C.: Design and implementation of the infrastructure of HadGEM3: the next-generation Met Office climate modelling system, *Geosci. Model Dev.*, 4, 223–253, doi:10.5194/gmd-4-223-2011, 2011. 443

Hoyle, C. R., Marécal, V., Russo, M. R., Allen, G., Arteta, J., Chemel, C., Chipperfield, M. P., D'Amato, F., Dessens, O., Feng, W., Hamilton, J. F., Harris, N. R. P., Hosking, J. S., Lewis, A. C., Morgenstern, O., Peter, T., Pyle, J. A., Reddman, T., Richards, N. A. D., Telford, P. J., Tian, W., Viciani, S., Volz-Thomas, A., Wild, O., Yang, X., and Zeng, G.: Representation of tropical deep convection in atmospheric models – Part 2: Tracer transport, *Atmos. Chem. Phys.*, 11, 8103–8131, doi:10.5194/acp-11-8103-2011, 2011. 451

Koch, D. and Del Genio, A. D.: Black carbon semi-direct effects on cloud cover: review and synthesis, *Atmos. Chem. Phys.*, 10, 7685–7696, doi:10.5194/acp-10-7685-2010, 2010. 439

Koch, D., Schulz, M., Kinne, S., McNaughton, C., Spackman, J. R., Balkanski, Y., Bauer, S., Berntsen, T., Bond, T. C., Boucher, O., Chin, M., Clarke, A., De Luca, N., Dentener, F., Diehl, T., Dubovik, O., Easter, R., Fahey, D. W., Feichter, J., Fillmore, D., Freitag, S., Ghan, S., Ginoux, P., Gong, S., Horowitz, L., Iversen, T., Kirkevåg, A., Klimont, Z., Kondo, Y., Krol, M., Liu, X., Miller, R., Montanaro, V., Moteki, N., Myhre, G., Penner, J. E., Perlwitz, J., Pitari, G., Reddy, S., Sahu, L., Sakamoto, H., Schuster, G., Schwarz, J. P., Seland, Ø., Stier, P., Takegawa, N., Takemura, T., Textor, C., van Aardenne, J. A., and Zhao, Y.: Evaluation of black carbon estimations in global aerosol models, *Atmos. Chem. Phys.*, 9, 9001–9026, doi:10.5194/acp-9-9001-2009, 2009. 440

Constraints on aerosol processes in climate models

Z. Kipling et al.

Title Page

Abstract

Introduction

Conclusions

References

Tables

Figures

◀

▶

◀

▶

Back

Close

Full Screen / Esc

Printer-friendly Version

Interactive Discussion



- Kunsch, H. R.: The jackknife and the bootstrap for general stationary observations, *Ann. Stat.*, 17, 1217–1241, 1989. 450
- Lin, S.-J. and Rood, R. B.: Multidimensional flux-form semi-Lagrangian transport schemes, *Mon. Wea. Rev.*, 124, 2046–2070, doi:10.1175/1520-0493(1996)124<2046:MFFSLT>2.0.CO;2, 1996. 446
- 5 Lohmann, U. and Feichter, J.: Global indirect aerosol effects: a review, *Atmos. Chem. Phys.*, 5, 715–737, doi:10.5194/acp-5-715-2005, 2005. 439
- Lohmann, U. and Hoose, C.: Sensitivity studies of different aerosol indirect effects in mixed-phase clouds, *Atmos. Chem. Phys.*, 9, 8917–8934, doi:10.5194/acp-9-8917-2009, 2009. 447
- 10 Lohmann, U., Feichter, J., Penner, J., and Leaitch, R.: Indirect effect of sulfate and carbonaceous aerosols: a mechanistic treatment, *J. Geophys. Res.*, 105, 12193–12206, doi:10.1029/1999JD901199, 2000. 439
- Lohmann, U., Stier, P., Hoose, C., Ferrachat, S., Kloster, S., Roeckner, E., and Zhang, J.: Cloud microphysics and aerosol indirect effects in the global climate model ECHAM5-HAM, *Atmos. Chem. Phys.*, 7, 3425–3446, doi:10.5194/acp-7-3425-2007, 2007. 447
- 15 Mann, G., Johnson, C. E., Bellouin, N., Dalvi, M., Abraham, L., Carslaw, K. S., Boucher, O., Stier, P., Rae, J., Spracklen, D. V., Telford, P., Pyle, J. A., O'Connor, F., Carver, G., Pringle, K. J., and Woodhouse, M. T.: Evaluation of the new UKCA climate–composition model – Part 3: Tropospheric aerosol properties, in preparation, 2012. 443
- 20 Mann, G. W., Carslaw, K. S., Spracklen, D. V., Ridley, D. A., Manktelow, P. T., Chipperfield, M. P., Pickering, S. J., and Johnson, C. E.: Description and evaluation of GLOMAP-mode: a modal global aerosol microphysics model for the UKCA composition-climate model, *Geosci. Model Dev.*, 3, 519–551, doi:10.5194/gmd-3-519-2010, 2010. 443, 444
- Mu, M., Randerson, J. T., van der Werf, G. R., Giglio, L., Kasibhatla, P., Morton, D., Collatz, G. J., DeFries, R. S., Hyer, E. J., Prins, E. M., Griffith, D. W. T., Wunch, D., Toon, G. C., Sherlock, V., and Wennberg, P. O.: Daily and 3-hourly variability in global fire emissions and consequences for atmospheric model predictions of carbon monoxide, *J. Geophys. Res.*, 116, D24303, doi:10.1029/2011JD016245, 2011. 451
- 25 Myhre, G., Samset, B. H., Schulz, M., Balkanski, Y., Bauer, S., Bernsten, T. K., Bian, H., Bellouin, N., Chin, M., Diehl, T., Easter, R. C., Feichter, J., Ghan, S. J., Hauglustaine, D., Iversen, T., Kinne, S., Kirkevåg, A., Lamarque, J.-F., Lin, G., Liu, X., Luo, G., Ma, X., Penner, J. E., Rasch, P. J., Seland, Ø., Skeie, R. B., Stier, P., Takemura, T., Tsigaridis, K., Wang, Z., Xu, L., Yu, H., Yu, F., Yoon, J.-H., Zhang, K., Zhang, H., and Zhou, C.: Radia-

Constraints on aerosol processes in climate models

Z. Kipling et al.

Title Page

Abstract

Introduction

Conclusions

References

Tables

Figures

◀

▶

◀

▶

Back

Close

Full Screen / Esc

Printer-friendly Version

Interactive Discussion



- 5 tive forcing of the direct aerosol effect from AeroCom Phase II simulations, *Atmos. Chem. Phys. Discuss.*, 12, 22355–22413, doi:10.5194/acpd-12-22355-2012, 2012. 439
- Nordeng, T. E.: Extended versions of the convective parameterization scheme at ECMWF and their impact on the mean and transient activity of the model in the tropics, Technical Memorandum 206, European Centre for Medium-Range Weather Forecasts, Reading, UK, 42 pp., 1994. 447
- O'Connor, F., Johnson, C., Morgenstern, O., Sanderson, M., Young, P., Collins, W., and Pyle, J.: Evaluation of the new UKCA climate-composition model – Part II: The troposphere, in preparation, 2012. 443
- 10 O'Connor, F. M., Carver, G. D., Savage, N. H., Pyle, J. A., Methven, J., Arnold, S. R., Dewey, K., and Kent, J.: Comparison and visualisation of high-resolution transport modelling with aircraft measurements, *Atmos. Sci. Lett.*, 6, 164–170, 2005. 449
- Penner, J. E., Chuang, C. C., and Liousse, C.: The Contribution of Carbonaceous Aerosols to Climate Change, in: *Nucleation and Atmospheric Aerosols 1996: Proceedings of the 14th International Conference on Nucleation and Atmospheric Aerosols*, Elsevier Sci., New York, 759–769, 1996. 439
- 15 Peters, K., Quaas, J., and Bellouin, N.: Effects of absorbing aerosols in cloudy skies: a satellite study over the Atlantic Ocean, *Atmos. Chem. Phys.*, 11, 1393–1404, doi:10.5194/acp-11-1393-2011, 2011. 439
- 20 Ramanathan, V. and Carmichael, G.: Global and regional climate changes due to black carbon, *Nature Geosci.*, 1, 221–227, doi:10.1038/ngeo156, 2008. 439
- Reddington, C. L., McMeeking, G., Mann, G. W., Coe, H., Frontoso, M. G., Liu, D., Flynn, M., Spracklen, D. V., and Carslaw, K. S.: The size distribution and mixing state of black carbon aerosol over Europe, *Atmos. Chem. Phys. Discuss.*, 12, 26503–26560, doi:10.5194/acpd-12-26503-2012, 2012. 440, 450
- 25 Riahi, K., Rao, S., Krey, V., Cho, C., Chirkov, V., Fischer, G., Kindermann, G., Nakicenovic, N., and Rafaj, P.: RCP 8.5 – a scenario of comparatively high greenhouse gas emissions, *Clim. Change*, 109, 33–57, doi:10.1007/s10584-011-0149-y, 2011. 446
- 30 Roeckner, E., Baeuml, G., Bonventura, L., Brokopf, R., Esch, M., Giorgetta, M., Hagemann, S., Kirchner, I., Kornblueh, L., Manzini, E., Rhodin, A., Schlese, U., Schulzweida, U., and Tompkins, A.: The atmospheric general circulation model ECHAM5. Part I: Model description, Report 349, Max Planck Institute for Meteorology, Hamburg, Germany, available from <http://www.mpimet.mpg.de>, 2003. 446

Constraints on aerosol processes in climate models

Z. Kipling et al.

Title Page

Abstract

Introduction

Conclusions

References

Tables

Figures

◀

▶

◀

▶

Back

Close

Full Screen / Esc

Printer-friendly Version

Interactive Discussion



- Schulz, M., Textor, C., Kinne, S., Balkanski, Y., Bauer, S., Bernsten, T., Berglen, T., Boucher, O., Dentener, F., Guibert, S., Isaksen, I. S. A., Iversen, T., Koch, D., Kirkevåg, A., Liu, X., Montanaro, V., Myhre, G., Penner, J. E., Pitari, G., Reddy, S., Seland, Ø., Stier, P., and Takemura, T.: Radiative forcing by aerosols as derived from the AeroCom present-day and pre-industrial simulations, *Atmos. Chem. Phys.*, 6, 5225–5246, doi:10.5194/acp-6-5225-2006, 2006. 439
- Schwarz, J. P., Gao, R. S., Fahey, D. W., Thomson, D. S., Watts, L. A., Wilson, J. C., Reeves, J. M., Darbeheshti, M., Baumgardner, D. G., Kok, G. L., Chung, S. H., Schulz, M., Hendricks, J., Lauer, A., Kärcher, B., Slowik, J. G., Rosenlof, K. H., Thompson, T. L., Langford, A. O., Loewenstein, M., and Aikin, K. C.: Single-particle measurements of midlatitude black carbon and light-scattering aerosols from the boundary layer to the lower stratosphere, *J. Geophys. Res.*, 111, D16207, doi:10.1029/2006JD007076, 2006. 441
- Schwarz, J. P., Spackman, J. R., Fahey, D. W., Gao, R. S., Lohmann, U., Stier, P., Watts, L. A., Thomson, D. S., Lack, D. A., Pfister, L., Mahoney, M. J., Baumgardner, D., Wilson, J. C., and Reeves, J. M.: Coatings and their enhancement of black carbon light absorption in the tropical atmosphere, *J. Geophys. Res.*, 113, D03203, doi:10.1029/2007JD009042, 2008. 439
- Schwarz, J. P., Spackman, J. R., Gao, R. S., Watts, L. A., Stier, P., Schulz, M., Davis, S. M., Wofsy, S. C., and Fahey, D. W.: Global-scale black carbon profiles observed in the remote atmosphere and compared to models, *Geophys. Res. Lett.*, 37, L18812, doi:10.1029/2010GL044372, 2010. 440, 442, 449, 452, 454
- Seinfeld, J. H. and Pandis, S. N.: *Atmospheric Chemistry and Physics: From Air Pollution to Climate Change*, Wiley-Interscience, 1998. 447, 467
- Sekhon, R. S. and Srivastava, R. C.: Doppler radar observations of drop-size distributions in a thunderstorm, *J. Atmos. Sci.*, 28, 983–994, doi:10.1175/1520-0469(1971)028<0983:DROODS>2.0.CO;2, 1971. 444
- Slinn, W.: Precipitation scavenging, in: *Atmospheric Science and Power Production*, edited by: Randerson, D., US Department of Energy, 1984. 444, 467
- Slinn, W. G. N.: Predictions for particle deposition to vegetative canopies, *Atmos. Environ.*, 16, 1785–1794, doi:10.1016/0004-6981(82)90271-2, 1982. 444, 467
- Spracklen, D. V., Pringle, K. J., Carslaw, K. S., Chipperfield, M. P., and Mann, G. W.: A global off-line model of size-resolved aerosol microphysics: I. Model development and prediction of aerosol properties, *Atmos. Chem. Phys.*, 5, 2227–2252, doi:10.5194/acp-5-2227-2005, 2005. 444

Constraints on aerosol processes in climate models

Z. Kipling et al.

Title Page

Abstract

Introduction

Conclusions

References

Tables

Figures

◀

▶

◀

▶

Back

Close

Full Screen / Esc

Printer-friendly Version

Interactive Discussion



- Stier, P., Feichter, J., Kinne, S., Kloster, S., Vignati, E., Wilson, J., Ganzeveld, L., Tegen, I., Werner, M., Balkanski, Y., Schulz, M., Boucher, O., Minikin, A., and Petzold, A.: The aerosol-climate model ECHAM5-HAM, *Atmos. Chem. Phys.*, 5, 1125–1156, doi:10.5194/acp-5-1125-2005, 2005. 444, 446
- 5 Stier, P., Seinfeld, J. H., Kinne, S., Feichter, J., and Boucher, O.: Impact of nonabsorbing anthropogenic aerosols on clear-sky atmospheric absorption, *J. Geophys. Res.*, 111, D18201, doi:10.1029/2006JD007147, 2006. 439
- Stier, P., Seinfeld, J. H., Kinne, S., and Boucher, O.: Aerosol absorption and radiative forcing, *Atmos. Chem. Phys.*, 7, 5237–5261, doi:10.5194/acp-7-5237-2007, 2007. 439
- 10 Stier, P., Grandey, B., West, R., Lohmann, U., Quaas, J., and Seinfeld, J. H.: Observational constraints on mechanistic aerosol–cloud coupling in the microphysical aerosol–climate model ECHAM–HAM, in preparation, 2012. 447
- Sundqvist, H., Berge, E., and Kristjánsson, J. E.: Condensation and cloud parameterization studies with a mesoscale numerical weather prediction model, *Mon. Wea. Rev.*, 117, 1641–1657, doi:10.1175/1520-0493(1989)117<1641:CACPSW>2.0.CO;2, 1989. 447
- 15 445
- Telford, P. J., Braesicke, P., Morgenstern, O., and Pyle, J. A.: Technical Note: Description and assessment of a nudged version of the new dynamics Unified Model, *Atmos. Chem. Phys.*, 8, 1701–1712, doi:10.5194/acp-8-1701-2008, 2008.
- 20 Telford, P. J., Abraham, N. L., Archibald, A. T., Braesicke, P., Dalvi, M., Morgenstern, O., O'Connor, F. M., Richards, N. A. D., and Pyle, J. A.: Implementation of the Fast-JX Photolysis scheme into the UKCA component of the MetUM chemistry climate model, *Geosci. Model Dev. Discuss.*, 5, 3217–3260, doi:10.5194/gmdd-5-3217-2012, 2012. 445, 449
- Textor, C., Schulz, M., Guibert, S., Kinne, S., Balkanski, Y., Bauer, S., Berntsen, T., Berglen, T., Boucher, O., Chin, M., Dentener, F., Diehl, T., Easter, R., Feichter, H., Fillmore, D., Ghan, S., Ginoux, P., Gong, S., Grini, A., Hendricks, J., Horowitz, L., Huang, P., Isaksen, I., Iversen, I., 25 Kloster, S., Koch, D., Kirkevåg, A., Kristjánsson, J. E., Krol, M., Lauer, A., Lamarque, J. F., Liu, X., Montanaro, V., Myhre, G., Penner, J., Pitari, G., Reddy, S., Seland, Ø., Stier, P., Takemura, T., and Tie, X.: Analysis and quantification of the diversities of aerosol life cycles within AeroCom, *Atmos. Chem. Phys.*, 6, 1777–1813, doi:10.5194/acp-6-1777-2006, 2006. 440, 455
- 30

**Constraints on
aerosol processes in
climate models**Z. Kipling et al.

[Title Page](#)[Abstract](#)[Introduction](#)[Conclusions](#)[References](#)[Tables](#)[Figures](#)[◀](#)[▶](#)[◀](#)[▶](#)[Back](#)[Close](#)[Full Screen / Esc](#)[Printer-friendly Version](#)[Interactive Discussion](#)

Tiedtke, M.: A comprehensive mass flux scheme for cumulus parameterization in large-scale models, *Mon. Wea. Rev.*, 117, 1779–1800, doi:10.1175/1520-0493(1989)117<1779:ACMFSF>2.0.CO;2, 1989. 447

Twomey, S.: The influence of pollution on the shortwave albedo of clouds, *J. Atmos. Sci.*, 34, 1149–1152, 1977. 439

van der Werf, G. R., Randerson, J. T., Giglio, L., Collatz, G. J., Kasibhatla, P. S., and Arellano Jr., A. F.: Interannual variability in global biomass burning emissions from 1997 to 2004, *Atmos. Chem. Phys.*, 6, 3423–3441, doi:10.5194/acp-6-3423-2006, 2006. 446, 451

van der Werf, G. R., Randerson, J. T., Giglio, L., Collatz, G. J., Mu, M., Kasibhatla, P. S., Morton, D. C., DeFries, R. S., Jin, Y., and van Leeuwen, T. T.: Global fire emissions and the contribution of deforestation, savanna, forest, agricultural, and peat fires (1997–2009), *Atmos. Chem. Phys.*, 10, 11707–11735, doi:10.5194/acp-10-11707-2010, 2010. 451

Vignati, E.: M7: an efficient size-resolved aerosol microphysics module for large-scale aerosol transport models, *J. Geophys. Res.-Atmos.*, 109, 1–17, doi:10.1029/2003JD004485, 2004. 443, 446

Wilcox, E. M.: Direct and semi-direct radiative forcing of smoke aerosols over clouds, *Atmos. Chem. Phys.*, 12, 139–149, doi:10.5194/acp-12-139-2012, 2012. 439

Wilson, D. R. and Ballard, S. P.: A microphysically based precipitation scheme for the UK meteorological office unified model, *Q. J. R. Meteorol. Soc.*, 125, 1607–1636, 1999. 443

Wilson, D. R., Bushell, A. C., Kerr-Munslow, A. M., Price, J. D., and Morcrette, C. J.: PC2: a prognostic cloud fraction and condensation scheme – Part I: Scheme description, *Q. J. R. Meteorol. Soc.*, 134, 2093–2107, 2008. 443

Wofsy, S. C., the HIPPO Science Team, and Cooperating Modellers and Satellite Teams: HIPPER Pole-to-Pole Observations (HIPPO): fine-grained, global-scale measurements of climatically important atmospheric gases and aerosols, *Philos. T. R. Soc. A*, 369, 2073–2086, doi:10.1098/rsta.2010.0313, 2011. 440

Woodward, S.: Modeling the atmospheric life cycle and radiative impact of mineral dust in the Hadley Centre climate model, *J. Geophys. Res.*, 106, 18155–18166, doi:10.1029/2000JD900795, 2001. 444

Zarzycki, C. M. and Bond, T. C.: How much can the vertical distribution of black carbon affect its global direct radiative forcing?, *Geophys. Res. Lett.*, 37, L20807, doi:10.1029/2010GL044555, 2010. 439

- Zhang, K., O'Donnell, D., Kazil, J., Stier, P., Kinne, S., Lohmann, U., Ferrachat, S., Croft, B., Quaas, J., Wan, H., Rast, S., and Feichter, J.: The global aerosol-climate model ECHAM-HAM, version 2: sensitivity to improvements in process representations, *Atmos. Chem. Phys.*, 12, 8911–8949, doi:10.5194/acp-12-8911-2012, 2012. 446
- 5 Zhang, L., Gong, S., Padro, J., and Barrie, L.: A size-segregated particle dry deposition scheme for an atmospheric aerosol module, *Atmos. Environ.*, 35, 549–560, doi:10.1016/S1352-2310(00)00326-5, 2001. 444, 467

Constraints on aerosol processes in climate models

Z. Kipling et al.

[Title Page](#)[Abstract](#)[Introduction](#)[Conclusions](#)[References](#)[Tables](#)[Figures](#)[I◀](#)[▶I](#)[◀](#)[▶](#)[Back](#)[Close](#)[Full Screen / Esc](#)[Printer-friendly Version](#)[Interactive Discussion](#)

Constraints on aerosol processes in climate models

Z. Kipling et al.

Title Page

Abstract

Introduction

Conclusions

References

Tables

Figures

⏪

⏩

◀

▶

Back

Close

Full Screen / Esc

Printer-friendly Version

Interactive Discussion



Table 1. Differences relevant to black carbon between the aerosol schemes in HadGEM3–UKCA and ECHAM5–HAM2, in their BASE configurations.

| Process | HadGEM3–UKCA | ECHAM5–HAM2 |
|-----------------------------------|--|---|
| Biofuel emission size | same as fossil fuel (60nm diameter) | same as biomass-burning (150nm diameter) |
| Fossil fuel and biofuel emissions | added to lowest level | applied as surface flux in vertical diffusion |
| Biomass-burning emission height | uniform in height over ~ 50m to 3km | biome-dependent (Dentener et al., 2006) |
| Ageing insoluble to soluble | 10 monolayers required | 1 monolayer required |
| Dry deposition | Slinn (1982); Zhang et al. (2001) operator-split | Ganzeveld et al. (1998) as surface flux in vertical diffusion |
| Below-cloud scavenging | Slinn (1984) | Seinfeld and Pandis (1998) |
| In-cloud nucleation scavenging | 100 % of soluble accumulation/coarse modes Rain only Immediate removal | Prescribed fractions of all modes Rain and snow Replaced where precipitation evaporates |
| Convective scavenging | Operator-split, acting on grid-box means | In-plume, acting on tracer fluxes |
| Aerosol feedbacks | Disabled | Enabled |

Table 2. Configurations and emissions used for model simulations of the HIPPO campaign. The inventory (GFED2 or GFED3.1) used for biomass-burning emissions is shown, along with the year for which these emissions are specified. Other emissions are taken from the AEROCOM Hindcast inventory, or (for additional gas phase emissions in UKCA) RCP 8.5.

| Model | Label | Description | Biomass-burning emissions |
|--------------|------------|--|---------------------------------|
| HadGEM3–UKCA | BASE | Basic configuration, with only diagnostic modifications for flight-track sampling. | GFED2 1997–2006 clim. (monthly) |
| | G3M | As BASE, but with GFED3.1 monthly biomass emissions. | GFED3.1 2008–2010 (monthly) |
| | CVSCAV | As BASE, but with in-plume convective scavenging scheme added, as described in the text. | GFED2 1997–2006 clim. (monthly) |
| | CVSCAV+G3M | Combining both in-plume convective scavenging (CVSCAV) and GFED3.1 emissions (G3M). | GFED3.1 2008–2010 (monthly) |
| ECHAM5–HAM2 | BASE | Basic configuration, with only diagnostic modifications for flight-track sampling. | GFED2 1997–2006 clim. (monthly) |
| | G3M | As BASE, but with GFED3.1 monthly biomass emissions using modified vertical distribution. | GFED3.1 2008–2010 (monthly) |
| | G3H | As BASE, but with GFED3.1 3-hourly biomass emissions using modified vertical distribution. | GFED3.1 2008–2010 (3-hourly) |

Constraints on aerosol processes in climate models

Z. Kipling et al.

Title Page

Abstract Introduction

Conclusions References

Tables Figures

◀ ▶

◀ ▶

Back Close

Full Screen / Esc

Printer-friendly Version

Interactive Discussion



Constraints on aerosol processes in climate models

Z. Kipling et al.

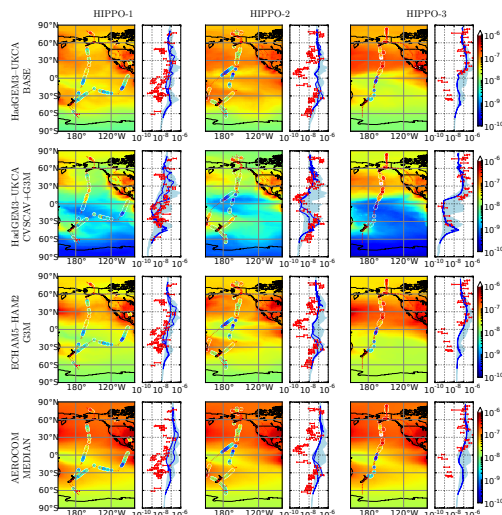


Fig. 1. Flight tracks for the first three phases of the HIPPO campaign (January 2009, October/November 2009 and March/April 2010 respectively). The circles show the BC burden (in kg m^{-2}) estimated from the HIPPO SP2 observations over each vertical profile, while the background shading shows the monthly-mean BC burden from the HadGEM3–UKCA (BASE and CVSCAV+G3M) and ECHAM5–HAM2 (G3M) simulations. The bottom row shows the burdens from the AEROCOM Phase I (Textor et al., 2006) median model (constructed from the ARQM, GISS, GOCART, GRANTOUR, KYU, LOA, MATCH, MPI_HAM, MOZGN, PNNL, UIO_CTM, UIO_GCM, ULAQ and UMI models). The side plots show the observed burdens (red bars, representing the range due to uncertainty in extrapolation of profiles to the surface and a 15 km lid, plus the 30% uncertainty in the mixing ratios used), the along-track model burden (blue line, two-valued due to the southbound and northbound legs) and the zonal range of the model burden between the map edges (shading).

[Title Page](#)
[Abstract](#)
[Introduction](#)
[Conclusions](#)
[References](#)
[Tables](#)
[Figures](#)
[Back](#)
[Close](#)
[Full Screen / Esc](#)
[Printer-friendly Version](#)
[Interactive Discussion](#)

Constraints on aerosol processes in climate models

Z. Kipling et al.

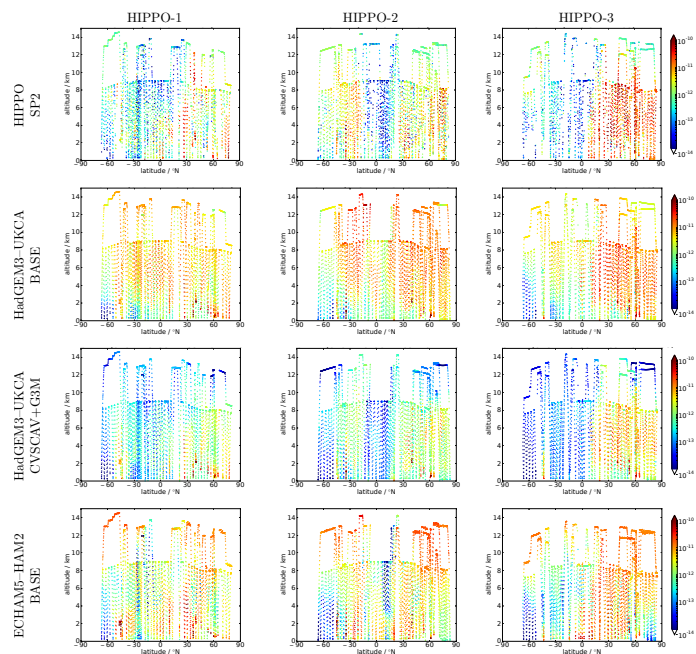


Fig. 2. Mass mixing ratio of BC in the atmosphere, from each phase of the HIPPO campaign, calculated by aggregating SP2 data over 1-min intervals, and from nudged HadGEM3–UKCA (BASE and CVSCAV) and ECHAM5–HAM2 (BASE) simulations, sampled along the HIPPO flight track (also at 1-min intervals).

Title Page

Abstract

Introduction

Conclusions

References

Tables

Figures

◀

▶

◀

▶

Back

Close

Full Screen / Esc

Printer-friendly Version

Interactive Discussion



Constraints on aerosol processes in climate models

Z. Kipling et al.

Title Page

Abstract

Introduction

Conclusions

References

Tables

Figures

◀

▶

◀

▶

Back

Close

Full Screen / Esc

Printer-friendly Version

Interactive Discussion

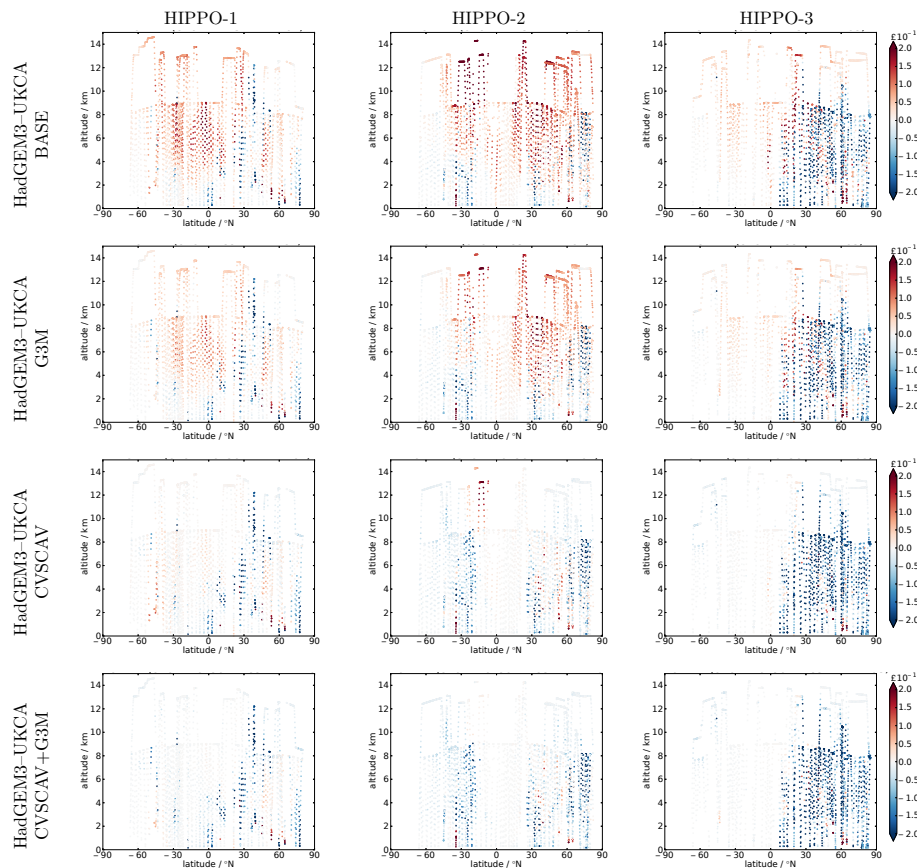


Fig. 3. Difference of BC mass mixing ratio simulated by HadGEM3–UKCA in each configuration (rows) from that observed during each phase of the HIPPO campaign (columns). The model is nudged and sampled along the HIPPO flight track at 1-min intervals; observed mixing ratio is calculated from HIPPO SP2 data aggregated over 1-min intervals.

Constraints on aerosol processes in climate models

Z. Kipling et al.

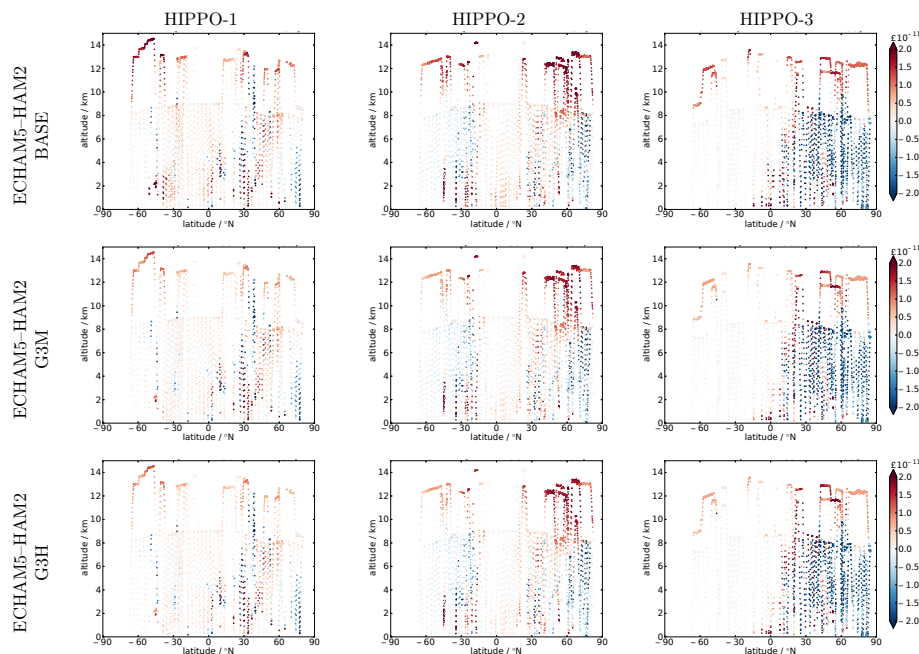


Fig. 4. Difference of BC mass mixing ratio simulated by ECHAM5–HAM2 in each configuration (rows) from that observed during each phase of the HIPPO campaign (columns). The model is nudged and sampled along the HIPPO flight track at 1-min intervals; observed mixing ratio is calculated from HIPPO SP2 data aggregated over 1-min intervals.

Title Page

Abstract

Introduction

Conclusions

References

Tables

Figures

◀

▶

◀

▶

Back

Close

Full Screen / Esc

Printer-friendly Version

Interactive Discussion



Constraints on aerosol processes in climate models

Z. Kipling et al.

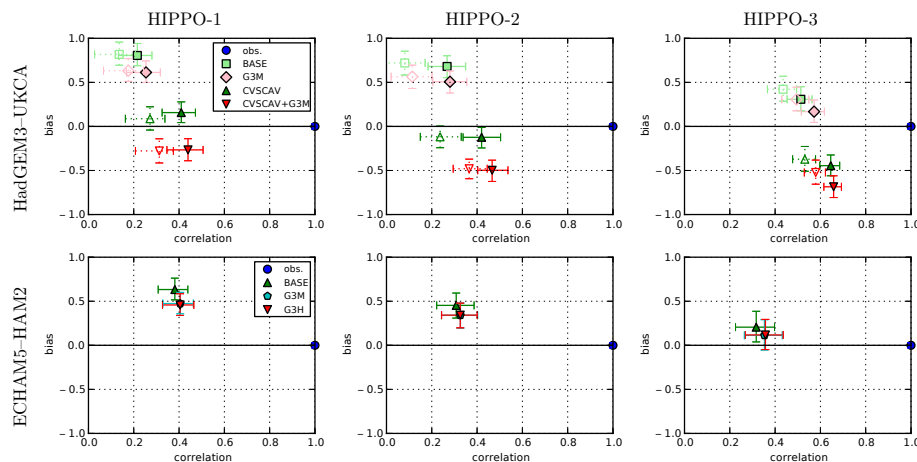


Fig. 5. Bias-correlation plots of $\log(\text{BC mass mixing ratio})$ between the HadGEM3–UKCA (top row) and ECHAM5–HAM2 (bottom row) simulations and each phase of the HIPPO campaign (columns). The error bars represent a 95% confidence interval based on a moving-block bootstrap and the $\pm 30\%$ error in the SP2-derived mixing ratios from HIPPO-1. The solid symbols represent nudged simulations, while the hollow symbols (for HadGEM3–UKCA) represent free-running simulations. The “obs.” point on the right-hand side indicates where a model which reproduces the observations perfectly would be located.

Title Page

Abstract

Introduction

Conclusions

References

Tables

Figures

◀

▶

◀

▶

Back

Close

Full Screen / Esc

Printer-friendly Version

Interactive Discussion

